



OPEN Impact of KDM6B mosaic brain knockout on synaptic function and behavior

Bastian Brauer^{1,7}, Carlos Ancatén-González^{2,3,7}, Constanza Ahumada-Marchant¹, Rodrigo C. Meza³, Nicolas Merino-Veliz¹, Gino Nardocci^{4,5}, Lorena Varela-Nallar^{1,6}, Gloria Arriagada¹, Andrés E. Chávez³✉ & Fernando J. Bustos^{1,6}✉

Autism spectrum disorders (ASD) are complex neurodevelopmental conditions characterized by impairments in social communication, repetitive behaviors, and restricted interests. Epigenetic modifications serve as critical regulators of gene expression playing a crucial role in controlling brain function and behavior. Lysine (K)-specific demethylase 6B (KDM6B), a stress-inducible H3K27me3 demethylase, has emerged as one of the highest ASD risk genes, but the precise effects of *KDM6B* mutations on neuronal activity and behavioral function remain elusive. Here we show the impact of KDM6B mosaic brain knockout on the manifestation of different autistic-like phenotypes including repetitive behaviors, social interaction, and significant cognitive deficits. Moreover, KDM6B mosaic knockout display abnormalities in hippocampal excitatory synaptic transmission decreasing NMDA receptor mediated synaptic transmission and plasticity. Understanding the intricate interplay between epigenetic modifications and neuronal function may provide novel insights into the pathophysiology of ASD and potentially inform the development of targeted therapeutic interventions.

Keywords KDM6B, ASD, Gene editing, NMDA, Behavior

Autism spectrum disorders (ASD) and neurodevelopmental disorders are a group of clinically heterogeneous conditions that are characterized by changes in social skills, attention deficits, hyperactivity and cognition. These disorders can cause difficulties with social communication and interaction, as well as restricted, repetitive, and stereotyped patterns of behavior¹. People with ASD often have co-occurring conditions including epilepsy, depression, anxiety, and hyperactivity², having significant impact on the individual's everyday life. The complexity and heterogeneity of ASD pathogenesis is mainly due to the large number of ASD-related genetic variations including copy number variants, single nucleotide polymorphism, deletions and duplications according to SFARI gene database³. Moreover, the target gene function is quite diverse leading to abnormalities in neuronal communication, cytoskeleton formation and dynamics, chromatin regulation, and gene expression^{4–8}. Over the last decade, special emphasis has been given to mutations in chromatin regulating genes where new gene variants have been described that could explain the genetic complexity of ASD⁹. However, the precise mechanisms through which these mutations contribute to ASD phenotypes remain largely elusive.

Several studies have focused on unraveling the role that mutations or knockout (KO) of chromatin associated genes have on the appearance of ASD phenotypes, including Chromodomain helicase DNA binding protein 8 (CHD8), Lysine demethylase 6A (KDM6A), and Lysine methyltransferase 2C (KMT2C)^{10–12}. Recently, one of the largest whole exome sequencing studies, showed that one of the highest risk genes for ASD is lysine demethylase 6b (KDM6B), also known as JMJD3 (Jumonji domain-containing protein-3)⁹. KDM6B functions as a histone tail demethylase specifically targeting histone H3 lysine 27 trimethylation (H3K27me3)¹³. In its role as a demethylase of H3K27, it counteracts the repressive function of the Polycomb repressive complex 2 (PRC2)¹⁴,

¹Constantine-Paton Research Laboratory, Instituto de Ciencias Biomédicas, Facultad de Medicina y Facultad de Ciencias de la Vida, Universidad Andres Bello, Santiago, Chile. ²Programa de Doctorado en Ciencias, Mención Neurociencia, Universidad de Valparaíso, Valparaíso, Chile. ³Instituto de Neurociencias, Centro Interdisciplinario de Neurociencia de Valparaíso (CINV), Facultad de Ciencias, Universidad de Valparaíso, 2340000 Valparaíso, Chile. ⁴School of Medicine, Faculty of Medicine, Universidad de los Andes, Santiago, Chile. ⁵Molecular Biology and Bioinformatics Lab, Program in Molecular Biology and Bioinformatics, Center for Biomedical Research and Innovation (CIIB), Universidad de Los Andes, Santiago, Chile. ⁶Millennium Nucleus of Neuroepigenetics and Plasticity (EpiNeuro), Santiago, Chile. ⁷These authors contributed equally: Bastian Brauer and Carlos Ancatén-González. ✉email: andres.chavez@uv.cl; fernando.bustos@unab.cl

thereby facilitating the induction of gene expression¹⁵. KDM6B has been widely studied for its role associated with cancer aggressiveness and progression, as well as its involvement in brain neurogenesis, neuron differentiation, maturation, survival, and in neurological disorders^{16–19}. Full KDM6B KO animals die at birth due to respiratory deficits²⁰, thus most studies have used conditional or heterozygous animals. Heterozygous KDM6B KO mice reportedly display hyperactivity, social and cognitive deficits²¹. However, the synaptic mechanisms underlying these observed behaviors were not investigated²¹. Using conditional KO in cerebellar granule neurons, it has been shown that the correct control and dynamics of H3K27me3 deposition is needed for neuronal maturation²². In addition, conditional knockout of KDM6B in excitatory neurons causes loss of synaptic activity, spine density, and synaptic vesicle number likely by dysregulation of VGLUT1/2 gene expression^{21,21}.

Given its critical role in regulating chromatin structure and gene transcription, dysregulation of KDM6B has been implicated in various neurodevelopmental disorders, including ASD^{21,24,25}. Human genetic studies have identified over 130 likely pathogenic rare variants in the *KDM6B* gene, highlighting its significance in neurodevelopment, however only 3 confirmed variants with ASD phenotype have been validated³. Notably, studies of more than 85 variants across the *KDM6B* gene in humans have shown a myriad of phenotypes. However, a common denominator in all of them is the presence of cognitive deficits²⁶. This underscores the importance of gaining insight into the mechanisms and behavioral outcomes of KDM6B mutations and how they relate to autistic-like behaviors and brain function.

Here we utilized the CRISPR/Cas9 system delivered via AAV to create a whole-brain mosaic knockout (mKO) of *Kdm6b* at postnatal day 1, with the aim of investigating its role in controlling behavior and the functional consequence on synaptic mechanisms associated with these behaviors. As anticipated, KDM6B mKO animals exhibited reduced KDM6B expression, consequently leading to an increase in H3K27me3. Additionally, we observed hyperactivity, repetitive behaviors, social impairment, and cognitive deficits. Notably, these findings correlate with a significant impairment of synaptic plasticity in the hippocampus, and more specifically a significant disruption in NMDA receptor (NMDAR)-mediated excitatory post-synaptic currents, which may underlie the observed cognitive effects. Our results demonstrate the feasibility of modeling *Kdm6b* loss-of-function mutations using CRISPR/Cas9, providing an additional platform to study the cellular and molecular mechanisms underlying mutations associated with ASD.

Results

Editing of the *Kdm6b* gene to generate mosaic brain knockout

To elucidate the role of KDM6B in the pathogenesis of ASD, we employed the CRISPR/Cas9 system to knock out its expression in cultured neurons and animal brain, as previously described^{10,27,28}. We designed four sgRNAs targeting exon 6 of *Kdm6b* (Fig. 1A), considering its conservation across all isoforms. These sgRNAs (KDM6B KO1–4) were tested in cultured neurons from Cas9KI animals transducing with AAVs coding for CRISPR/Cas9 at 3 days in vitro (DIV). At 10 DIV, RT-qPCR from these neurons was conducted to assess KO efficiency revealing that all of them downregulated *Kdm6b* expression (Fig. 1B). KDM6B KO4 showed the best efficiency downregulating KDM6B expression in vitro by approximately 70%. Subsequently, we utilized this sgRNA to conduct our in vivo experiments.

To evaluate whether CRISPR/Cas9 induced *Kdm6b* KO produces autistic-like behaviors and explore potential underlying mechanisms, we utilized intracerebroventricular delivery of AAV encoding KDM6B KO4 and TdTomato as fluorescence marker to determine transduction efficiency. This methodology ensures efficient transduction of brain cells as previously described^{10,27,28}. Cas9KI animals received injections at P1 to produce KDM6B mKO, and behavioral testing started at eight weeks. For inclusion in the analyses, animals had to meet three criteria: 1. Display a widespread fluorescent label throughout the entire brain, 2. Exhibit a positive T7 endonuclease I assay confirming gene editing, and 3. Demonstrate a reduction in KDM6B expression of at least 50%. Nine control and KDM6B mKO animals met the criteria and were included in the final analyses. Following behavioral or electrophysiological analyses, animals were imaged to determine transduction efficiency, revealing widespread transduction including CA1, CA3 and DG in the hippocampus (Fig. 1C). Using hippocampal tissue from transduced animals, the T7 endonuclease I assay for gene editing showed that all nine KDM6B mKO animals were positive for editing at the locus (Fig. 1D). Furthermore, RT-qPCR revealed that transduced animals exhibited an approximate 70% reduction in mRNA levels (Fig. 1E), and western blot analyses of mKO animals show a significant reduction in KDM6B protein expression (Fig. 1F). In addition, digital PCR assay shows a significant reduction in the number of copies of KDM6B cDNA in hippocampal tissue of KDM6B mKO animals (Fig. 1G), confirming the reduction of the expression of *Kdm6b* after gene editing.

KDM6B is an enzyme responsible for catalyzing histone H3 lysine 27 demethylation, leading to the activation of gene targets, counteracting the repressive role of the PRC2 complex^{13,15}. Consequently, we hypothesized that knocking out *Kdm6b* would result in an increase in total H3K27me3 in brain tissue. As anticipated, our observations confirmed that KDM6B mKO animals exhibit a global increase in this histone tail modification (Fig. 1H–I). These results indicate that our strategy targeting *Kdm6b* can efficiently reduce its expression in the entire brain and consequently increase global H3K27me3.

KDM6B mKO animals show hyperactivity and repetitive behaviors

It has been demonstrated that heterozygous KDM6B animals exhibit behaviors resembling those observed in ASD, including reduced anxiety²¹. Furthermore, studies using KDM6B conditional KO animals have shown impaired memory but no signs of anxiety²³. Our approach to knocking out KDM6B in the animal brain to produce KDM6B mKO helps us study behaviors and could help shed light on the mechanisms behind KDM6B loss-of-function mutations. Eight weeks after infection, both control (tdTomato injected) and KDM6B mKO animals were subjected to a battery of behavioral tests. First, we examined the locomotion activity of KDM6B

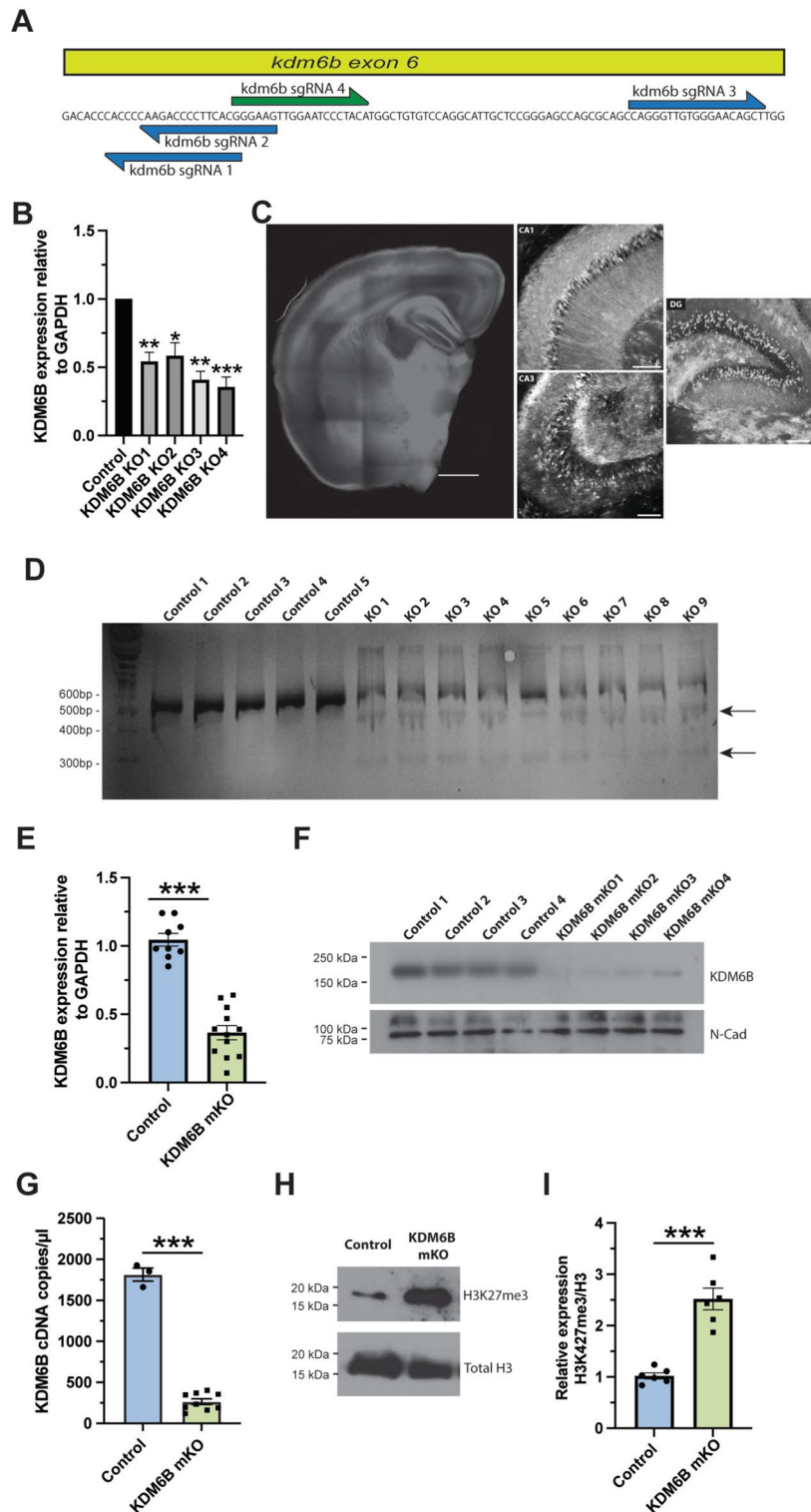


Fig. 1. Knockout of *Kdm6b* by gene editing. **(A)** Scheme showing exon 6 of *Kdm6b* genomic sequence and the position where the designed sgRNAs bind to the genomic sequence. In green is sgRNA-4 that is used for all in vivo experiments. **(B)** Cultured cortical neurons were transfected with sgRNAs and Cas9 to determine sgRNA efficiency. At 10 DIV RT-qPCR was conducted to determine expression levels of KDM6B relative to GAPDH. **(C)** Representative image of brain slice and high magnification of CA1, CA3 and DG of the hippocampus after transduction by intracerebroventricular injection of CRISPR/Cas9. **(D)** T7 endonuclease I assay from transduced cortical tissue of injected animals. **(E)** RT-qPCR to determine expression levels of KDM6B relative to GAPDH in transduced cortical tissue of injected animals. **(F)** Representative western blot of KDM6B and N-Cadherin as loading control in WT and KDM6B mKO animals. **(G)** Digital PCR assay to determine KDM6B cDNA copies/ μ l in WT and KDM6B mKO animals (WT n = 3; KDM6B mKO n = 9) **(H)** Representative image of western blot analysis of total H3 histone, and H3K27me3. **(I)** Quantification of the relative expression of H3K27me3 from cortical tissue extracted from 6 control or KDM6B mKO animals. Bars represent mean \pm SEM; * $p < 0.05$, ** $p < 0.01$, *** $p < 0.001$. Student's t-test was used to determine significance compared to control condition. Scale bar = 1000 μ m and 100 μ m for high magnification images.

mKO animals using the accelerated rotarod apparatus. We found that KDM6B mKO animals spent more time on the rotarod than control animals (Fig. 2A). The presence of anxiety-like behaviors is recognized as a distinctive feature in both human and animal cases of ASD^{1,10,27,29,30}. Therefore, we investigated whether KDM6B mKO animals exhibited this phenotype. Using the open field test, we allowed the animals to freely explore for 10 min and measured their location and movements in the arena (Fig. 2B). Like the rotarod test, KDM6B mKO animals traveled a significantly longer distance than control animals in the arena (Fig. 2C). However, KDM6B mKO animals spent a similar amount of time than control animals in the center of the arena (Fig. 2D) and in the periphery (Fig. 2E), indicating that KDM6B mKO animals do not exhibit anxiety behaviors. To confirm this finding, we conducted the light and dark, and zero maze tests. In the light–dark apparatus, animals were placed in the dark box and allowed to explore for 10 min (Fig. 3A). The test revealed no differences in total entries (Fig. 3B) or time spent (Fig. 3C) in the illuminated zone between KDM6B mKO and controls. However, we did find a significant difference in the distance traveled in the illuminated zone (Fig. 3D). Moreover, in the zero maze (Fig. 3E), KDM6B mKO and control animals spent a similar amount of time in the open zone (Fig. 3F) but KDM6B mKO mice exhibited an increased number of entries to the open zone compared to control animals (Fig. 3G). Such difference can be attributed to the hyperactivity displayed by the animals, leading them to cover longer distances and enter open zones more frequently. Then, animals underwent the marble burying test to assess repetitive behaviors and anxiety where KDM6B mKO animals buried a significantly greater number of marbles compared to control animals (Fig. 3H). Lastly, when grooming episodes were quantified, KDM6B mKO animals displayed a significantly higher count of grooming episodes compared to control animals (Fig. 3I). Altogether these findings suggest that KDM6B mKO animals exhibit limited anxiety as shown in the marble burying test and in addition animals show significant hyperactivity and repetitive behaviors.

KDM6B mKO animals exhibit deficiencies in social behaviors

Given that individuals with ASD commonly face challenges in social interaction, often demonstrating a deficit or lack of proficiency in engaging socially^{1,29}, we sought to assess the social interaction capabilities of KDM6B mKO mice. We started by analyzing the behavior of animals in the tube dominance test to determine social hierarchy and interaction between animals. Test revealed that KDM6B mKO animals win the challenge significantly more times than the control animals in days 1–4 (Fig. 4A), showing an increase in social dominance behavior. Next, we employed the 3-chamber social interaction test to assess the capacity for social interaction, allowing the animals to interact in the chambers for 10 min. While control animals spent a greater amount of time interacting with the novel animal compared to the object, KDM6B mKO animals spent similar amounts of time interacting with both the novel animal and the object (Fig. 4B), indicating a social deficit in mutant mice. To better understand

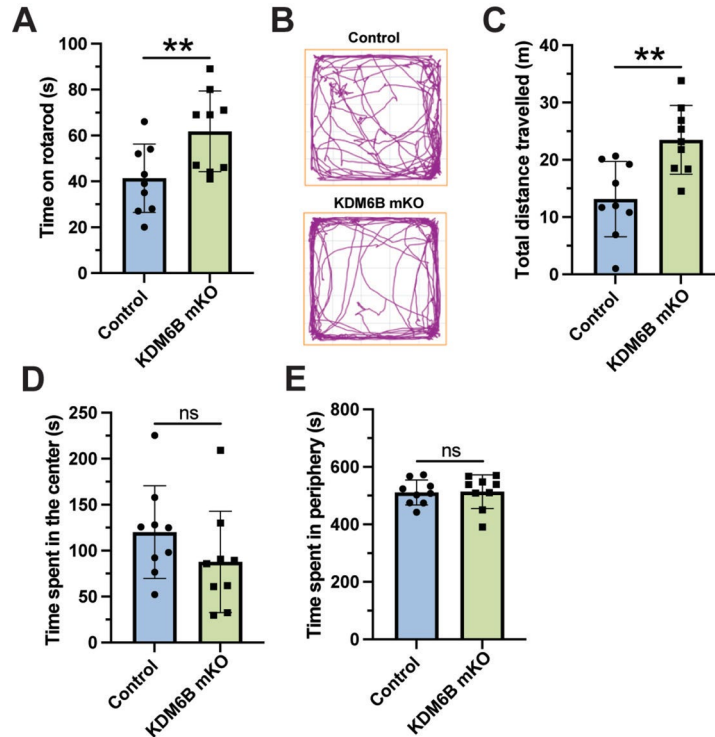


Fig. 2. Hyperactivity in KDM6B mKO animals. (A) Time spent on the rotarod apparatus. (B) Representative trace plots of open field test in Control and KDM6B mKO animals. (C–E) Quantification of the total distance travelled (C), time spent in the center area (D), time spent in the periphery (E). Bars represent mean ± SEM. Student's t-test was used to determine significance compared to control condition. ** $p < 0.01$, $n = 9$ animals for Control and KDM6B mKO animals. ns = non-significant.

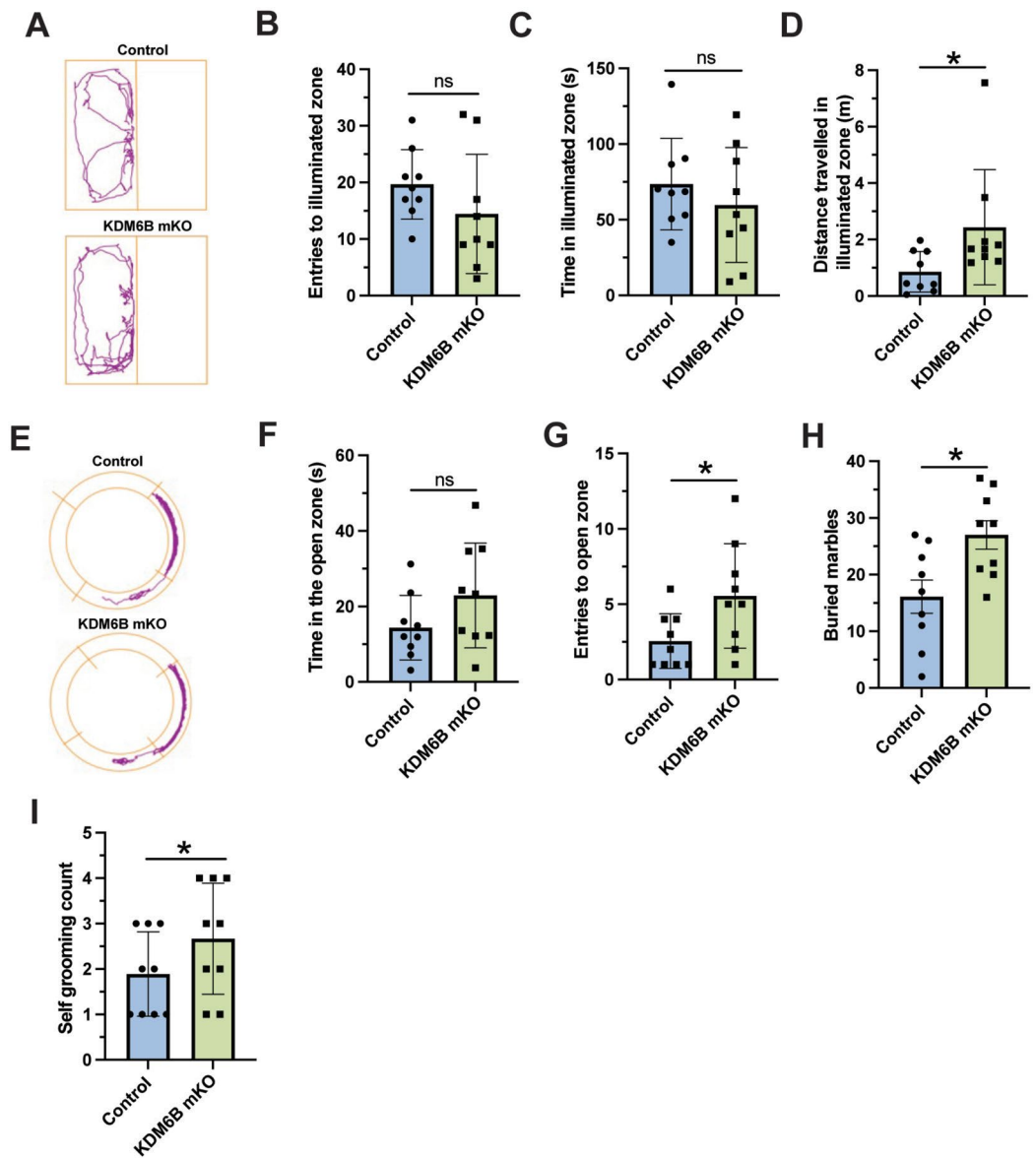


Fig. 3. KDM6B mKO animals display repetitive behaviors. (A) Representative trace plots of dark and light test (top = Control; bottom = KDM6B mKO). (B–D) Quantification of the number of entries to illuminated zone (B), the time spent in the illuminated zone (C), and the distance travelled in the illuminated zone (D). (E) Representative trace plots of the zero-maze test (top = Control; bottom = KDM6B mKO). (F–G) Quantification of the time spent in the open zone (F), and the total entries to the open zone (G) in the zero maze. (H) Quantification of the number of marbles buried during the marble burying test. (I) Quantification of the self-grooming behavior shown by Control or KDM6B mKO animals. Bars represent mean \pm SEM. Student's t-test was used to determine significance compared to control condition. * $p < 0.05$, $n = 9$ animals for Control and KDM6B mKO animals. ns = non-significant.

the social deficits observed in the 3-chamber test, we employed the direct social interaction paradigm. During this test, KDM6B mKO and control animals were given the opportunity to interact within a clear box for 10 min, and their interactions were recorded for evaluation. Specifically, we focused on observing sniffing and grooming behaviors during this time. Our analysis revealed that social sniffing between animals showed no significant differences in nose–nose (N–N) interactions (Fig. 4C) or nose–head (N–H) interactions (Fig. 4D). However, upon evaluating nose–anogenital (N–A), a significant decrease in KDM6B mKO animals was observed (Fig. 4E), demonstrating a reduction in social investigative activity. Together, this data demonstrates that KDM6B mKO animals show increased social dominance and exhibit social deficits, as evidenced by decreased social interaction with other animals and behaviors indicative of avoiding direct interaction, as observed in the direct social interaction paradigm.

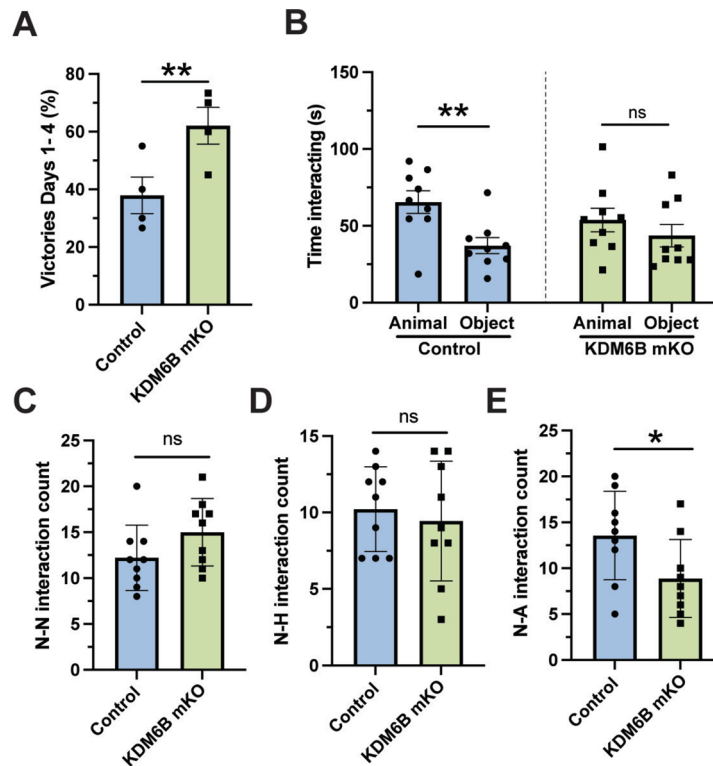


Fig. 4. Impaired social behaviors of KDM6B mKO animals. **(A)** Quantification of the number of victories in the tube dominance test. Each point represents the mean of victories per day 1–4. **(B)** Quantification of the time spent in the 3-chamber social interaction test with the novel animal or novel object in Control and KDM6B mKO animals. **(C–E)** Direct social interaction test to quantify **(C)** nose-nose (N–N), **(D)** nose-head (N–H), and **(E)** nose-anogenital (N–A) interactions between Control or KDM6B mKO animals. Bars represent mean \pm SEM. Student's *t*-test was used to determine significance compared to control condition. * $p < 0.05$, ** $p < 0.01$, $n = 9$ animals for Control and KDM6B mKO animals. ns = non-significant.

Impaired cognitive function in KDM6B mKO mice

Human patients with mutations in *KDM6B* have exhibited varying degrees of intellectual disability^{21,24,25}. Moreover, studies involving knockdown of the *Drosophila* ortholog of KDM6B and KDM6A, UTX, which plays a similar role in removing H3K27me3, have shown that deficits in UTX lead to cognitive impairments²⁶. Consequently, we investigated whether KDM6B mKO animals display deficits in memory formation. To assess spatial learning and memory, we employed the Barnes maze paradigm³¹. Measuring the total distance traveled by the animals over 5 days revealed that KDM6B mKO animals covered a longer distance each day in the apparatus compared to control animals (Fig. 5A). This aligns with our previous observations in the rotarod, open field apparatus, and light–dark test, highlighting the hyperactivity of KDM6B mKO animals. Additionally, we analyzed the time it took for the animals to find the escape hole for the first time, termed primary latency. KDM6B mKO animals experienced difficulties locating the escape hole, resulting in a greater primary latency in all days compared to control animals (Fig. 5B). To evaluate spatial memory formation, the escape hole was removed, and we monitored the time the animals spent in the zone of interest where the escape hole was previously located. We found that KDM6B mKO animals spent significantly less time in the zone of interest, indicating cognitive deficits (Fig. 5C). Lastly, we assessed long-term memory formation using the contextual fear conditioning paradigm. During the 5 min test period, KDM6B mKO animals exhibited a significantly reduced percentage of time freezing compared to control animals (Fig. 5D). Collectively, our data indicate that KDM6B mKO animals display severe cognitive impairments.

NMDA receptor mediated synaptic function and plasticity are diminished in KDM6B mKO mice

To investigate the physiological consequences of KDM6B ablation in brain function, we used acute brain slices from KDM6B mKO animals to perform an electrophysiological characterization of excitatory synaptic activity at the Schaffer–collateral to CA1 synapse in the hippocampus (Fig. 6A). We first characterized spontaneous AMPA receptor (AMPA)-mediated excitatory synaptic activity and found a significant decrease in the frequency but not in the amplitude of spontaneous excitatory postsynaptic currents (sEPSCs) in KDM6B-deficient synapses compared to control (Fig. 6B). Likewise, a significant decrease in the frequency of miniature excitatory postsynaptic currents (mEPSCs) was observed in KDM6B-deficient synapses (Fig. 6C), suggesting that ablation of KDM6B impacts spontaneous excitatory synaptic activity. To further determine whether KDM6B mKO impacts

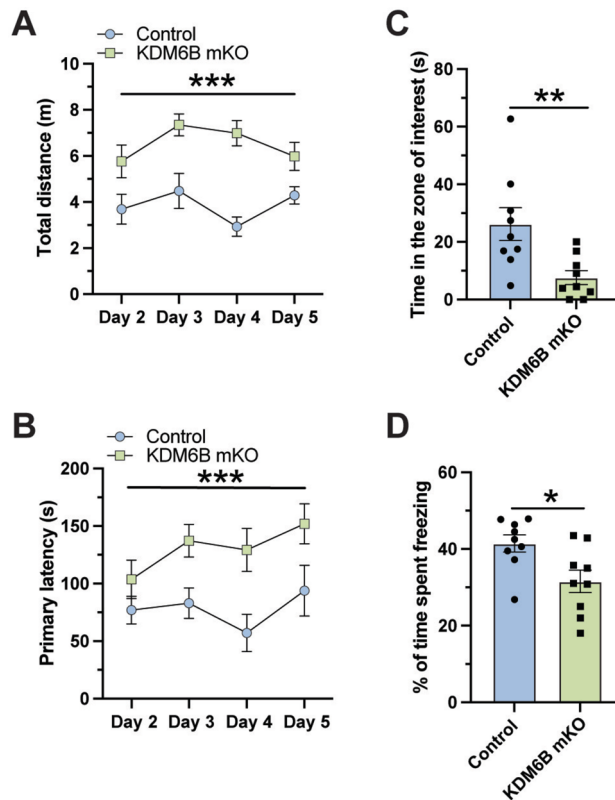


Fig. 5. KDM6B mKO animals display cognitive deficits. **(A)** Quantification of the total distance travelled in the Barnes maze apparatus. **(B)** Primary latency of Control and KDM6B mKO animals in the Barnes maze apparatus. **(C)** Quantification of the time spent in the zone of interest where the escape hole was formerly located. **(D)** Percentage of time spent freezing by Control and KDM6B mKO animals in the contextual fear conditioning test. Bars represent mean \pm SEM. Student's t-test was used to determine significance compared to control condition. * $p < 0.05$, ** $p < 0.01$, *** $p < 0.001$, $n = 9$ animals for Control and KDM6B mKO animals.

evoked neurotransmitter release probability, we perform paired-pulse ratio measurements at different interstimulus intervals. No differences between control and KDM6B mKO animals were observed (Fig. 6D), suggesting normal release probability in KDM6B-deficient synapses compared to control synapses. Moreover, no differences between control and KDM6B mKO animals were observed in AMPAR-mediated fEPSP input–output function (Fig. 6E), indicating that KDM6B ablation does not affect evoked glutamate release probability and AMPAR-mediated synaptic transmission in the hippocampus.

Next, we analyzed NMDAR/AMPA ratios by recording AMPAR-mediated EPSCs at -60 mV and isolated NMDAR-mediated EPSCs at $+40$ mV in the continuous presence of $10 \mu\text{M}$ NBQX (Fig. 7A). A significant decrease in the NMDAR/AMPA ratio was observed in KDM6B mKO deficient synapse compared to control (Fig. 7A), suggesting a decrease in the total number of NMDARs. To confirm this possibility, we measure isolated NMDAR-EPSCs input–output curve and found a significant decrease in KDM6B mKO compared to control animals (Fig. 7B). Moreover, we found that NMDAR-EPSC display significantly slower decay kinetics in KDM6B mKO mice (Fig. 7C), which could reflect a change in synaptic NMDAR subunit composition^{32–34}. To test this possibility, we first analyzed the expression of the NMDA receptor subunits NR2A and NR2B in hippocampal tissue using digital PCR. We found a significant reduction in the number of copies of NR2A cDNA (Fig. 7D) and an increase in the number of copies of NR2B cDNA (Fig. 7E) in hippocampal tissue of KDM6B mKO animals compared to control. Second, we performed electrophysiological recording of isolated NMDARs-EPSCs and used Ro25-6981 (500 nM) to selectively block NR2B-containing NMDARs. We found that NMDAR-EPSCs in KDM6B mKO mice were more sensitive to Ro25-6981 than controls mice (Fig. 7F). Altogether these results strongly suggest that KDM6B ablation alters NMDAR-mediated synaptic transmission by decreasing the total number and the subunit composition of NMDAR present at the Schaffer-collateral to CA1 synapse.

Due to the widespread infection in the animal brain, we also analyzed the effect of KDM6B mKO on synaptic function from layer V pyramidal neurons in the medial prefrontal cortex (Supplementary Fig. 1). As in the hippocampus, we found a significant decrease in the frequency but not in the amplitude of sEPSC in KDM6B-deficient synapses compared to control (Supplementary Fig. 1). Moreover, NMDAR-mediated EPSC recorded from KDM6B mKO animals are more sensitive to Ro25-6981 than control cells (Supplementary Fig. 1B), consistent with the idea that KDM6B mKO impact synaptic function and NMDARs subunit composition in both the cortex and the hippocampus.

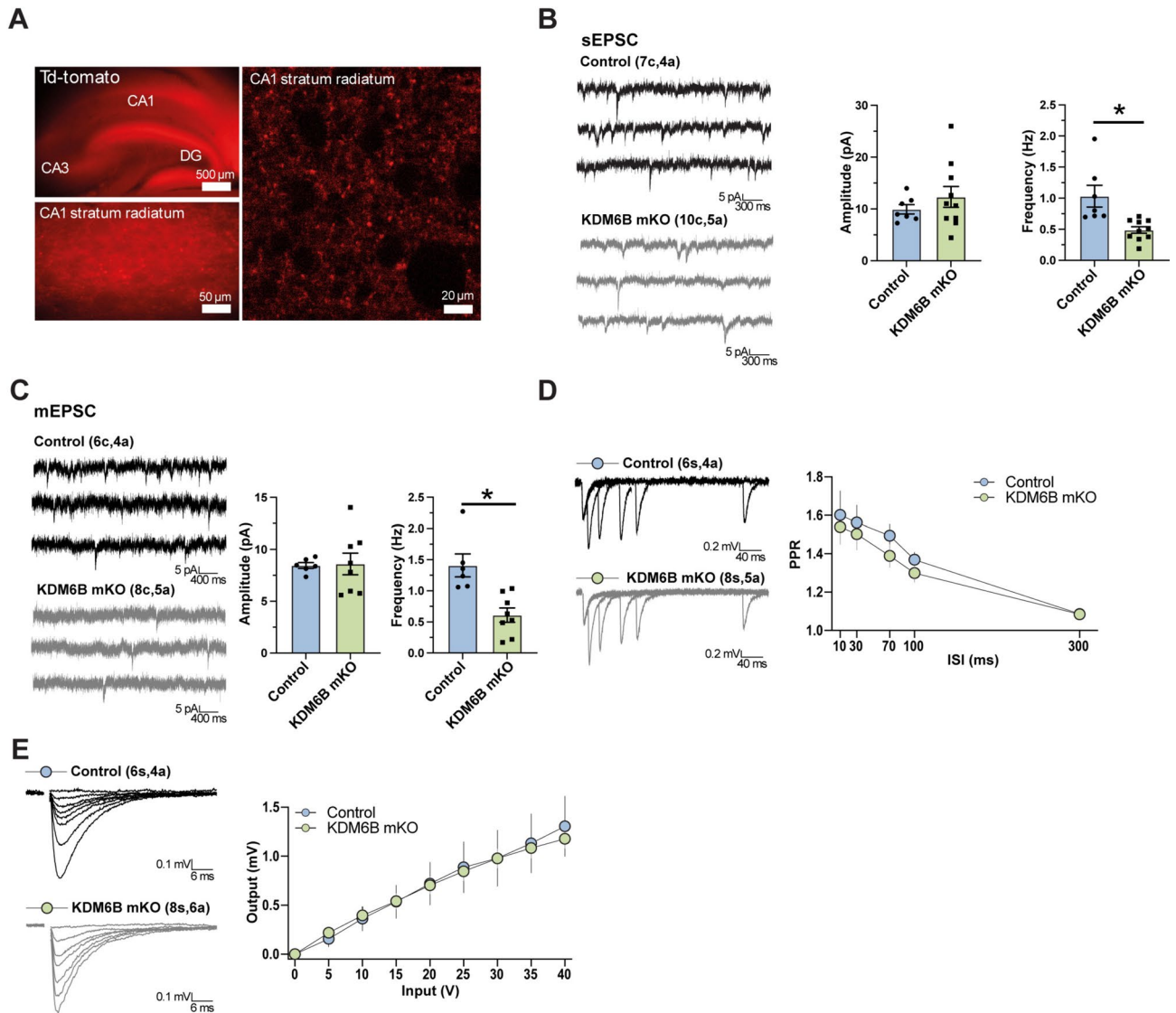


Fig. 6. AMPAR-mediated excitatory transmission is normal at hippocampal Sch–CA1 synapses in KDM6B mKO mice. **(A)** Representative image of acute hippocampal slice showing the expression of Td-tomato as infection control for KDM6B mKO in the hippocampus and in the CA1 field. **(B)** Representative AMPAR-mediated sEPSC traces (left) and summary plots (right) showing a decrease in frequency (Control: 1.03 ± 0.46 Hz vs KDM6B mKO: 0.48 ± 0.05 Hz, $p = 0.03$) but no in the amplitude of AMPAR-sEPSC in KDM6B mKO neurons. **(C)** Loss of KDM6B also significantly decrease the frequency (Control: 1.41 ± 0.2 Hz vs KDM6B mKO: 0.61 ± 0.11 Hz, $p = 0.03$) but not the amplitude of mEPSC. **(D)** Representative traces (left) and summary data (right) showing that ablation of KDM6B did not alter AMPAR-mediated paired-pulse ratio (PPR) measured at 10, 30, 70, 100, and 300 ms interstimulus intervals (ISI) or **(E)** input–output function. In all panels, summary data represent the mean \pm SEM. Number of cells (c), slices (s), and animals (a) are indicated in parentheses. Student t-test was used for statistical analysis, $*p < 0.05$.

Changes in NMDARs function has been associated with alteration in the induction of NMDAR-dependent long-term potentiation (NMDAR-LTP;³⁴). Thereby, we evaluated if NMDAR-LTP is altered by the ablation of KDM6B and found a strong reduction in the magnitude of LTP in KDM6B mKO mice compared to control (Fig. 7G). These results indicate that KDM6B plays an important role in NMDAR-dependent synaptic plasticity in the hippocampus likely by regulating NMDAR expression and activity.

Discussion

Although numerous ASD-related genetic variations are reported, we aimed to deepen our understanding of the role of KDM6B in regulating chromatin structure and gene transcription in the pathophysiology of ASD by investigating its effects on behavior and synaptic function. KDM6B is a lysine demethylase responsible for removing methyl groups from histone H3 lysine 27¹³, thereby counteracting the repressive effects of the PRC2¹⁴ hence facilitating gene expression. In agreement with previous reports in cKO KDM6B²³ and heterozygous

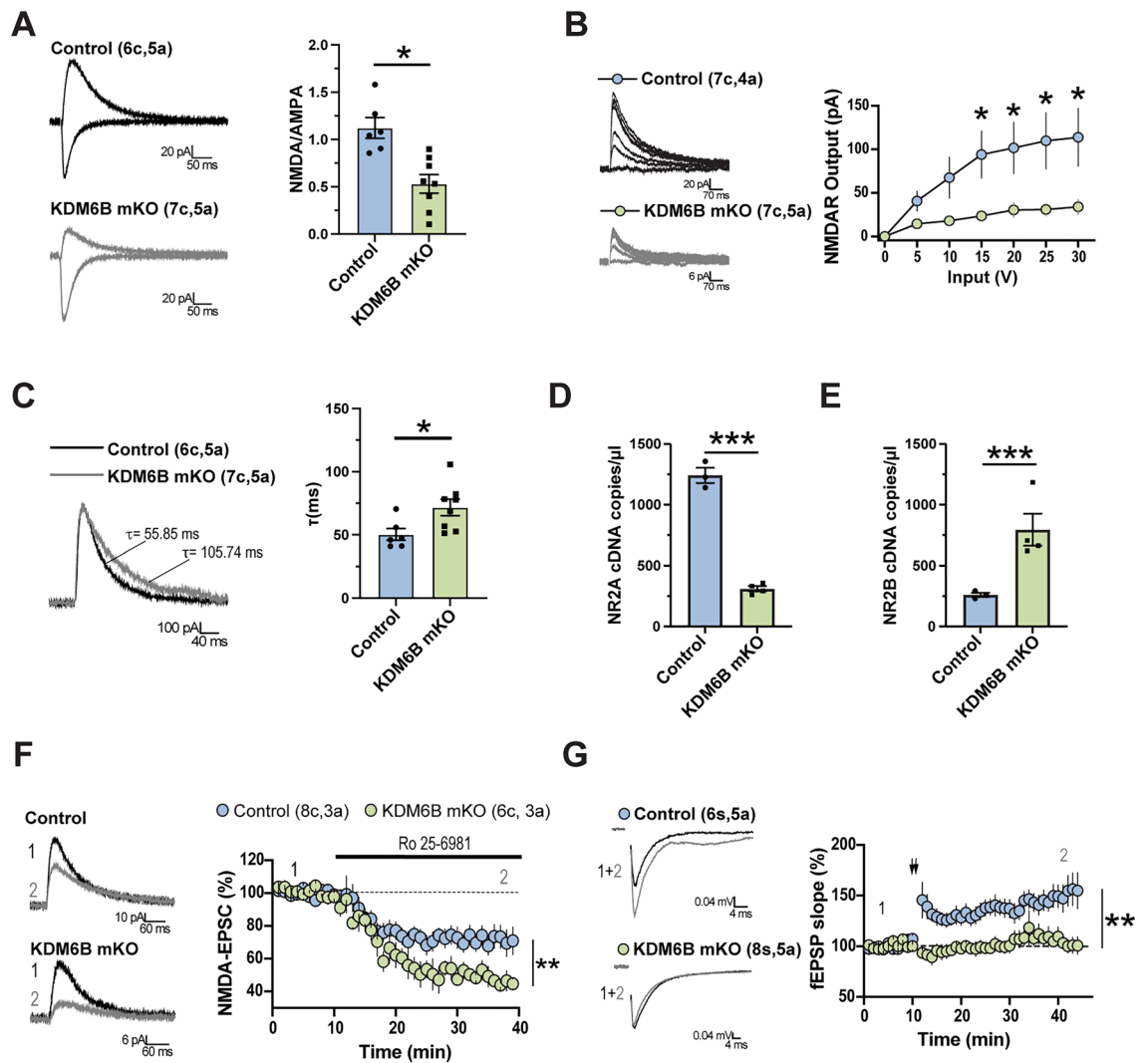


Fig. 7. NMDAR-mediated synaptic transmission is altered at hippocampal Sch-CA1 synapses in KDM6B mKO mice. **(A)** Representative traces (*left*) and summary data (*right*) showing that the NMDA/AMPA ratio is lower in KDM6B mKO compared to control (Control, 1.12 ± 0.10 ; KDM6B mKO, 0.53 ± 0.09 , $p = 0.02$). **(B)** NMDAR-EPSC input output curve is decrease in KDM6B mKO compared to control. **(C)** Normalized NMDAR-EPSCs (*left*) and summary data (*right*) showing slower NMDAR decay kinetics in KDM6B mKO compared with control (Control, 50.30 ± 11.30 ; KDM6B mKO, 71.70 ± 18.36 , $p = 0.04$). **(D-E)** Digital PCR assay to determine NR2A **(D)** or NR2B **(E)** cDNA copies/ μ l in WT and KDM6B mKO animals (WT $n = 3$; KDM6B mKO $n = 4$). **(F)** Averaged NMDAR-EPSCs (*left*) and summary data (*right*) showing more sensitivity to the selective NR2B antagonist Ro25-6981 (500 nM) in KDM6B mKO animals compared to control (Control, 71.24 ± 4.67 ; KDM6B mKO, 44.69 ± 4.65 , $p = 0.002$) **(G)** Representative traces (*left*) and summary data (*right*) showing that NMDA-dependent LTP induced by high frequency stimulation (arrows) is impaired in KDM6B mKO compared with control animal. Averaged sample traces were taken at times indicated by numbers in the summary plot. In all panels, summary data represent the mean \pm SEM and the number of cells (c), and animals (a) are indicated in parentheses. Student t-test was used for statistical analysis, * $p < 0.05$, ** $p < 0.01$, *** $p < 0.001$.

KDM6B KO animals²¹, our findings reveal that ablation of brain KDM6B play a critical role in controlling different ASD phenotype including hyperactivity, repetitive behaviors, social interaction, and cognitive deficits. Synaptic dysfunction is suggested as a core mechanism underlying ASD pathophysiology³⁵. Accordingly, our results demonstrated that ablation of KDM6B strongly impact NMDAR-mediated synaptic function and plasticity in the hippocampus, an observation that could explain the cognitive impairments observed in KDM6B mKO animal. These findings highlight a critical role of KDM6B in the pathophysiology of ASD phenotypes.

Here we utilized CRISPR/Cas9-mediated gene editing to generate KDM6B mKO animals, allowing us to investigate the behavioral and synaptic consequences of KDM6B deficiency, similarly to what we have previously done for KMT2C, a histone methyltransferase associated to ASD¹⁰. Genetic editing of *Kdm6b* leads to an enrichment of H3K27me3, reflecting the deficiency of KDM6B in cells. This dysregulation of histone methylation suggests a potential mechanism by which KDM6B deficiency may disrupt normal gene expression patterns.

Specifically, the increased H3K27me3 levels observed after gene editing likely result in the aberrant silencing of genes that are normally upregulated by KDM6B-mediated demethylation, as it has been shown in cerebellar granule neurons where KDM6B deficiency show deficient expression of genes needed for synaptic maturation, including the predominant NMDA receptor subunit *Grin2c*³⁶.

The behavioral characterization of the mKO animals reveals the absence of anxiety, as evidenced by results from the open field, light and dark, and zero maze tests. Surprisingly, in tests such as the rotarod and those previously mentioned, KDM6B mKO animals exhibited increased locomotion, traveling a longer distance compared to control animals. Given the absence of anxiety-related behaviors, this heightened activity can be attributed to hyperactivity in the animals, a trait reminiscent of observations in heterozygous KDM6B animals²¹. In contrast to findings in *Kdm6b* heterozygous models, our model system reveals the manifestation of repetitive behaviors observed in the marble burying and grooming tests. These differences might be a consequence of the different approach used to induce KDM6B KO and the extent of KO in different brain areas and cell types. Notably, KDM6B mKO animals also exhibit significant social impairments, a hallmark trait associated with ASD phenotypes that has also been observed in human patients carrying *KDM6B* mutations²⁵.

Although *KDM6B* mutants in humans have highly variable phenotypes, all of them present cognitive deficits as a common feature²⁶. In agreement, KDM6B mKO animals display cognitive deficits, as evidenced by impairments in spatial learning and memory formation in the Barnes maze and fear conditioning paradigms. These findings are in line with existing genetic studies in both humans and mice, which have implicated KDM6B in intellectual disability and cognitive impairment^{21,24,25,37}. It is worth highlighting that, contrary to previous observations, our study did not identify differences between male and female mice in terms of behavioral outcomes, thus all our data shows the average obtained from both sexes. This discrepancy could potentially be attributed to differences in methodology, including the approach used to induce gene editing in both alleles, as opposed to haploinsufficiency observed in KDM6B heterozygous models.

To gain insight into the mechanisms by which KDM6B deficiency produced autistic-like behaviors, we conducted electrophysiological recording from acute hippocampal slices as this region is mainly implicated in cognitive function. We found that KDM6B mKO has a significant reduction on the frequency of excitatory postsynaptic currents, however the amplitude was not changed, similarly to what has been observed in other ASD models including *TSC2*³⁸, *CNTNAP2*, and *AHI1*³⁹. Furthermore, we looked deeper into the impact on AMPAR-mediated synaptic transmission, revealing no significant differences compared to control animals. However, a significant reduction in the AMPAR/NMDAR ratio, indicating a decrease in the total number of NMDAR at the synapse was found in KDM6B mKO. This characteristic aligns with observations from other animal models of ASD, where a reduction in NMDAR expression has been documented including neuroligin-1 (*NL1*) and *Shank2* mutants^{40,41}. To determine the extent to which NMDARs affect synaptic transmission in KDM6B mKO animals, we induced NMDAR-dependent LTP and found that its induction is severely impaired. This phenomenon has been observed in other ASD animal models such as *TSC2*³⁸, *NL1*⁴⁰, and *Shank2*⁴¹ mutants among others⁴².

In addition, our experiments also show that the decay time of NMDA currents is significantly slower in KDM6B mKO animals in both the hippocampus and medial prefrontal cortex, suggesting a change in the subunit composition of the NMDARs from the faster NR2A subunit to the slower NR2B kinetics^{32,43}. This was supported by digital PCR analyses showing that NR2A subunit expression is reduced while NR2B subunit expression is increased. Future experiments will try to unravel the mechanisms behind this change in NMDA currents.

It has been demonstrated that NMDARs composed of the NR2A subunit are preferentially anchored by PSD95 to the postsynaptic site, whereas NR2B-composed NMDARs are anchored by SAP102^{44–47}. As the expression of PSD95 is regulated by H3K27me3^{48,49}, it is possible to suggest a link between KDM6B deficiency and altered PSD95 expression. Since PSD95 serves as the primary anchor for NR2A at the postsynaptic density, the absence of KDM6B may disrupt the expression of PSD95, consequently impacting the localization of NR2A/PSD95 complexes. Therefore, the disruption of KDM6B function may lead to an imbalance in NMDAR subunit composition, thereby influencing synaptic transmission and plasticity. Alternatively, it has been shown that NMDAR subunits expression during post-natal development is regulated by H3K27me3⁵⁰, thus KDM6B deficiency may directly affect the expression of NMDAR subunits impacting synaptic transmission and plasticity. These aspects warrant further investigations.

Our use of CRISPR/Cas9 to induce a mosaic knockout of KDM6B leads to a significant reduction in KDM6B expression, likely occurring across a wide range of brain cells as the approach we used is not cell-type specific. As we are unable to differentiate between cell types or confirm complete knockout in all targeted cells, we acknowledge that our experimental design does not allow us to definitively determine whether the observed effects are cell-autonomous (neurons) or non-cell-autonomous (e.g. mediated by KDM6B KO in glial cells). Moreover, it is possible that these effects may arise from a combination of cell-autonomous and non-cell-autonomous mechanisms. For instance, the disruption of KDM6B in one cell type could indirectly affect neighboring cells and contribute to the overall phenotype. This limitation is inherent in our approach and should be considered when interpreting our findings. To address this limitation in future studies, more refined techniques such as single-cell RNA sequencing or cell-type-specific knockouts would be required to elucidate the precise contributions of cell-autonomous versus non-cell-autonomous effects.

In conclusion, our approach and mouse model successfully recapitulated the phenotypes observed in humans, shedding light on the mechanisms through which KDM6B deficiency contributes to ASD phenotypes. Consequently, targeting NMDARs as a therapeutic strategy to address KDM6B brain deficiencies could pave the way for novel treatments for neurodevelopmental disorders resulting from *KDM6B* mutations.

Methods

Primary neuronal cultures

Postnatal day 1 Cas9 KI mice (C57BL/6J; JAX 026179) were euthanized by decapitation and the whole brain was extracted in ice cold Ca²⁺/Mg²⁺-free Hank's balanced salt solution (HBSS). Meninges were removed, the tissue was minced and incubated with Papain (20 U) for 15 min at 37 °C. Cells were rinsed twice with HBSS, resuspended by mechanical agitation through fire-polished glass Pasteur pipettes of decreasing diameters, and plated over poly-L-lysine-coated culture plates or cover slips. Cultures were maintained at 37 °C in 5% CO₂ in growth media [Neurobasal-A (Life technologies 1088802) supplemented with B27 (Life technologies 17504044), 2 mM L-glutamine (Life technologies 25030-081), 100 U/ml penicillin/streptomycin (Life technologies 15070-063)]. Half of the media was replaced every 3 days. Neuronal cultures were transduced at 3 days in vitro (DIV) using concentrated AAV particles.

Animals and injections

All animal procedures and experiments were performed according to the NIH and ARRIVE guidelines and were approved by the animal ethics committee from Universidad Andrés Bello (020/2018). Newborn Cas9 KI mice (C57BL/6J; JAX 026179) were cryoanesthetized in a cold aluminum plate and injected with 1 µL of concentrated AAV (1 × 10¹¹ vg), containing sgRNA or empty vector, in each cerebral ventricle at a depth of 3 mm in the animal's head at 2/5 of the intersection between lambda and the eye with a 10 µL HAMILTON syringe (Hamilton, 7653-01) and a 32 G needle (Hamilton, 7803-04). After the injection, P1 mice were placed in an infrared heating pad until they recovered their color and temperature, then they were returned to their cage with the mother^{10,51,52}. Three weeks after birth, mice from both conditions were weaned off and separated by sex in cages with a 12/12 light/dark cycle with free access to food and water. A chip (p-chips, Pharmaseq) was put in the tail of each animal for easy tracking during behavioral test. Behavior tests were performed between 9:00 am and 6:00 pm. At the end of the battery of behavioral tests, the animals were euthanized using isoflurane for subsequent molecular analyses.

Plasmids

For the expression of CRISPR/Cas9, plasmids were generated in AAV backbones. For sgRNAs 20nt target sequences were selected contiguous to a 5'-NGG protospacer-adjacent motif (PAM). sgRNAs for *Kdm6b* were designed against exon 6. sgRNA used for in vivo experiments (5' GGGAAAGTTGGAATCCCTACA 3') were cloned into a custom AAV plasmid under the control of the U6 promoter, and coding for tdTomato under the control of the human synapsin1 promoter, as in¹⁰. For viral packaging we used a plasmid coding for the PHP.eB capsid and pAdDeltaF6 plasmid to express adenovirus E4, E2A and VA genes. pUCmini-iCAP-PHP.eB was a gift from Viviana Gradinaru (Addgene plasmid # 103005; <http://n2t.net/addgene:103005>; RRID: Addgene_103005), pAdDeltaF6 was a gift from James M. Wilson (Addgene plasmid # 112867; <http://n2t.net/addgene:112867>; RRID: Addgene_112867).

AAV Production

AAVs were prepared as in^{10,27}. Briefly, AAV particles coding for sgRNA against *Kdm6b* under the control of a U6 promoter, together with the red fluorescent protein tdTomato controlled by the hSyn1 promoter were packed using the PHP.eB capsid to obtain high titer viral particles^{10,27,49,53}. HEK 293T were transfected with PEI and PHP.eB capsid plasmids, the vector with *Kdm6b* sgRNA-tdTomato, and the helper plasmid DF6. After 24 h of transfection, the media was replaced for DMEM 1% FBS. 72 h later, medium was collected from the plates and replaced with fresh DMEM 1% FBS. The collected medium was stored at 4 °C. To collect the viruses, 120 h after transfection, the cells were detached from the plate and transferred to 250 mL conical tubes, as well as the collected media. They were centrifuged for 10 min at 2000g, the supernatant was removed and saved for later use. The pellet was resuspended in SAN digestion buffer (5 mL of 40 mM Tris, 500 mM NaCl and 2 mM MgCl₂ pH 8.0) containing 100U/mL of Salt Active Nuclease (SAN) from Arcticzymes and incubated at 37 °C for 1 h. To the supernatant that was saved, a 5 × stock solution of 40% PEG 8000 (Sigma Aldrich, USA) in 2.5M NaCl was added, incubated on ice for 2 h and centrifuged at 4000g for 30 min in 250 mL bottles. The supernatant was collected and was placed in an Optiprep gradient and ultracentrifuged at 41.000g for 4 h. The phase containing the AAV was recovered and frozen at -80 °C for later use.

Genomic DNA extraction and T7 endonuclease I assay

Genomic DNA from transduced brain tissue was extracted using Quick-DNA Miniprep Kit (Zymo Research, USA) following manufacturer recommendations. To test *Kdm6b* edition, PCR with primers encompassing the edited region (5' CAGGCATTTCTCTCCAGTC 3', 5' GCAAAGGGCAGAGGAAGATT 3') were used. PCR products were run in agarose gels and purified by Gel extraction kit (Qiagen). 300 ng of amplified gDNA was used for T7 endonuclease I assay (NEB Cat#M0302). Assays were run in TBE polyacrylamide gels and visualized using Gel Red (Biotium).

RNA extraction and RT-qPCR

RNA was isolated from the tissues using TRIzol (Life Technologies, USA) according to manufacturer's instructions as in^{10,27,48,49}. To obtain complementary DNA (cDNA), 400 ng of RNA was used with iScript cDNA synthesis kit (Biorad, USA). Quantification was performed by qPCR using 3 µL of the cDNA mix, 6 µL Fast Evagreen qPCR Master Mix (Biotium, 31003). The relative abundance was measured by the ddCt method using the GAPDH gene as housekeeping control. Transcript detection was performed with specific primers for messenger RNA (mRNA):

Kdm6b: Fw 5' TGAAGAACGTCAAGTCCATTGTG 3'; Rv 5' TCCCGCTGTACCTGACAGT 3'; *Gapdh*: Fw 5' ATGGTGAAGTTCGGTGTGAA 3'; Rv 5' CATTCTCGGCCTTGACTGTG 3'.

Digital PCR (dPCR)

Undiluted cDNA was used for dPCR detection using a Qiaucuity One dPCR system (Qiagen, Germany). An 8.5K 24-well Qiaucuity Nanoplate was used to detect KDM6B, NR2A, NR2B, and GAPDH as reference control for even cDNA content. dPCR was run for 2 min at 95 °C for activation, 15 s 95 °C denaturation, 15 s 60 °C annealing, 15 s 72 °C extension for 40 cycles. Imaging was set to 500 ms exposure and gain of 4. For *Kdm6b* and *Gapdh* the same primers as in qPCR were used. In addition, primers used for dPCR were: *Grin2b* Fw 5' GCCAAACTGGAA GAACATGG 3'; Rv 5' TCTGCTCAGACTCTCACCCC 3'; *Grin2a* Fw 5' TGGAAGCTCCAAACTGGAAG 3'; Rv 5' CCTCACAGACTTTCATCCCC 3'.

Nuclear protein extraction

Nuclear extracts were used to determine histone tail modification by western blot as in¹⁰. Briefly, tissues were washed with cold PBS, centrifuged at 5000 g for 5 min and the pellet was resuspended in 5 volumes of cell lysis buffer (50 mM Hepes pH 7.9, 3 mM MgCl₂, 20 mM KCl, 0.1% NP-40, 1 mM DTT and protease inhibitor cocktail) and incubated on ice for 10 min. Solution was homogenized with 30 strokes in a dounce homogenizer and centrifuged at 6000 g for 15 min at 4 °C to separate the cytosolic and nuclear fractions. The pellet was resuspended in 1 volume of Buffer C (10 mM Hepes pH 7.9, 420 mM NaCl, 1.5 mM MgCl₂, 25% Glycerol, 0.2 mM EDTA, 1 mM DTT and protease inhibitor cocktail) and incubated for 1 h. Extracts were sonicated at 50% amplitude in cycles of 30 s ON/ 30 s OFF, centrifuged at 12,000g for 15 min at 4 °C. Supernatant was recovered and frozen at –80 °C to be subsequently quantified by Bradford.

Western blot analysis

Nuclear fractions or total extracts were separated on polyacrylamide gels and transferred to PVDF membranes (Millipore, USA). Membranes were blocked using 5% milk or 3% BSA and incubated overnight at 4 °C with primary antibodies. After rinsing, the membranes were incubated with secondary antibodies for 30 min at room temperature, rinsed and developed using chemiluminescence (Cell Signaling Technology, USA). Primary antibodies used: KDM6B (Sigma-Aldrich, 07-1533), N-Cadherin (Santa Cruz Biotechnology, SC-7939), H3K27me3 (Sigma-Aldrich, 07-449), and H3pan (Diagenode C15410324). For detection HRP-conjugated secondary antibodies were used (Cell Signaling Technology, USA).

Behavioral overview

All behavioral tests on mice were carried out 8 weeks after AAV injection as in^{10,27,28}. Before each test, mice cages were transported to the behavior room and habituated for 30 min in the dark. After completing a test, equipment and devices used were cleaned with 70% ethanol. Tests were recorded and analyzed with ANY-Maze software (Stoelting, USA).

Rotarod: Mice were placed on an elevated accelerating rod for three trials. Each trial lasted for a maximum of 3 min, during which the Rotarod underwent a linear acceleration of 4 rpm per min. Mean time and speed from each animal were registered before falling off.

Open Field: Mice were tested in an open field (45 × 45 cm) virtually divided into central and peripheral regions with ANY-Maze software. Apparatus was illuminated from above with 300 lx in center and 250 lx in periphery. Animals were allowed to roam freely for 10 min. The total distance traveled and time in center and periphery were analyzed.

Light and Dark: The apparatus used for this test is a 40 cm box split in half with 390 lx on light side and 0–2 lx on the dark side. Mice were placed in the dark chamber and were allowed to freely explore both chambers for 10 min. Distance traveled, time spent and number of entrances to the light side were analyzed.

Elevated zero-maze: The apparatus consisted of a 46 cm diameter circular runway and raised 54 cm off the ground. The runway was divided equally into four alternating quadrants of open arcs and closed arcs, with 15 cm walls. Mice started in the center of an open arm and were recorded by video tracking for 10 min. Measures of cumulative open and closed arc times, total open arm entries, distance in each arm and total distance traveled were analyzed.

Marble burying test: Mice were tested in a 45 × 45 cm box filled with 5 cm deep wood chips and 49 marbles distributed in a 7 × 7 pattern. Animals were placed in the test cage and allowed to explore and bury the marbles during a 30 min session that was videotaped. At the end of the session the subject was removed and the number of marbles buried (2/3 marble covered by wood chip) were counted.

Contextual fear conditioning: Equipment consisted of a sound attenuating box, fan, light (visible/I.R.), a speaker, a USB camera, a single on-board controller, and a mouse cage. All trials were recorded, and all mice underwent a habituation, conditioning and testing phase. During the habituation (day 1): mice were placed in the fear conditioning cage to explore freely for 5 min and then returned to their cage. During the conditioning phase (day 2): subject mouse was placed in the fear conditioning cage, let explore freely for 2 min and then subjected to an electric shock of 0.75 mA for 2 s. Next, animal was allowed to explore freely for 3 min and returned to its cage. On the test phase (day 3): Twenty-four hours after the conditioning phase, the animals were tested for contextual memory. Each mouse was placed in the fear conditioning box, allowed to freely explore for 5 min, and returned to its cage. The number and time of freezing episodes was registered.

Barnes Maze: A non-reflective gray circular platform (91 cm diameter) with 20 holes (5 cm diameter) evenly distributed along the perimeter, with one hole containing a metal escape tunnel was used. Three exogenous visual cues (length/width ~ 30 cm) were used around the platform: black circle, blue triangle and a yellow square.

The light was adjusted to 1000 lx in the center of the platform. All animals underwent a phase of habituation, spatial acquisition and testing³¹. For habituation (day 1): each mouse was placed in the center of the platform, directed towards the escape hole, and allowed to remain there for 1 min. Then it was taken and allowed to freely explore the maze for 5 min and was again allowed to spend 1 min inside the escape hole. If the mouse did not enter within 5 min, it was gently guided near the escape hole selected randomly on the table. During training phase (day 2–4): each animal was introduced into the start box, left in the center of the platform for 10 s and the start box was removed, and simultaneously a 16,000 Hz sound was played. The test ended at 3 min or when the mouse has found the escape hole. This procedure was repeated 2 times per day. During those days the following was recorded: Primary latency: Time to review the escape hole for the first time; Time in the zone of interest; Total distance traveled. In the test phase (day 5): the position of the escape tunnel was changed, and the animal was brought in the start box to the center of the platform, left for 10 s and sound reproduction was started. The test ended at 90 s or when the mouse found the escape tunnel. The number of primary and total errors, primary and total latency, and total distance before finding the gap were recorded. The number of visits to each hole was also measured to show preference.

Three-Chamber Sociability and Social Novelty Test: This was performed in a transparent acrylic three-chambered apparatus with the following dimensions: 61.5 × 43.5 × 22 cm. Each outer chamber was 20 × 43.5 cm. We used small cages of 8 cm diameter and 18 cm height to put the social (unknown WT mice of the same sex and similar age) and nonsocial stimulus (plastic block of 8 × 4 × 4 cm). A 20 lx illumination was used in this test. On the habituation phase (day 1): stimulus holders were placed in the center of outer chambers. The subject mouse was placed in the central chamber and allowed to explore freely for 10 min. Apparatus and stimulus holders were cleaned between mice with 70% ethanol. During pre-test (day 2): two clean paper balls were prepared and introduced inside each stimulus holder. The mouse was placed in the central chamber and allowed to explore freely for 10 min. Apparatus and stimulus holders were cleaned between mice with 70% ethanol. For the social preference test (day 3): a control mouse was placed in a stimulus holder to be used as a social stimulus and changed for another one every 2 test runs to avoid burnout or social fatigue⁵⁴. A plastic block was placed in the stimulus holder as a nonsocial stimulus. Once social and nonsocial objects were put in the outer chambers, mouse was placed in the central chamber and allowed to explore freely for 10 min. Behavior was video recorded. Time amount and distance traveled in the social and nonsocial chamber was registered, as well as the interaction time with each stimulus. Discrimination index was calculated by $(\text{time with novel animal} - \text{time with novel object}) / (\text{time with novel animal} + \text{time with novel object})$.

Social Interactions: In this test, an animal from the control condition or KDM6B mKO with a control animal of the same sex and similar age, were placed in a 30 × 30 × 30 cm box for 10 min. Social interactions (nose-nose sniffing, nose-face, nose-anogenital area, and grooming) between them were quantified.

Tube dominance: Tube test apparatus consisted of a smooth transparent acrylic tube of 30 cm length and internal diameter of 2.5 cm. Mice were habituated for 3 days. On day 1, each animal interacted and explored the tube freely for 30 min. On day 2 and 3, tube inlet was closed, and gel food was placed at the end. Animals were allowed to explore freely for 30 min. On the training phase (day 4 and 5) mice were taken by the tail and allowed to freely explore for approximately 1 min on the table where the tube was located. Then they were taken from the tail and put on one end of the tube and when the animal entered the tail, it was released. If the animal did not move for several seconds, it was gently prodded with a wooden stick. This step was repeated 5 times per side, so that the mouse passed through the tube a total of 10 times. The same procedure was repeated on day 4 and 5. On the test phase (day 6–9): two mice, one control and one KDM6B mKO, were taken and brought to the ends of the tube by the tail. When they entered completely and reached the middle of the tube, their tails were released to begin the confrontation. The test was repeated for 4 days. The mouse that pushes and removes its opponent from the tube was considered the winner and the one that is removed from the tube was considered the loser. All confrontations were video recorded to analyze the times each animal won and lost. The test stopped when the loser had all 4 paws out of the tube. The total number of wins and the number of wins per day were compared between control and KDM6B mKO conditions.

Brain sectioning and mounting

To assess brain transduction, after behaviors animals were deeply anesthetized, and half of the brain was extracted and fixed by immersion in PBS + 4% PFA + 4% Sucrose into 30 mL flasks for 24 h. After fixation, a Leica VT1000s vibratome was used to cut 100 μm coronal sections. Slices were kept in PBS and mounted using Fluoromont G (EMS, Hatfield, PA) to preserve the fluorescence signal. Brain images were captured with a Nikon Eclipse TE2000 epifluorescence microscope (Nikon, USA) or a Nikon C2 plus confocal microscope (Nikon, USA).

Slice electrophysiology

Acute coronal hippocampal slices (400 μm thick) were prepared from control and KDM6B mKO at postnatal day (P) 30 to P45 as previously described^{27,30,49,55,56}. Animal handling and use was conducted following a protocol approved by the Animal Care and Use Committee of the Universidad de Valparaíso (CBC 92-2023) in accordance with the bioethics regulation of the Chilean Research Council (ANID). Briefly, the brain was isolated and cut using a DKT vibratome in a solution containing the following (in mM): 215 sucrose, 2.5 KCl, 26 NaHCO₃, 1.6 NaH₂PO₄, 1 CaCl₂, 4 MgCl₂, 4 MgSO₄, and 20 glucose. After 30 min recovery, slices were incubated in an artificial CSF (ACSF) recording solution containing the following (in mM): 124 NaCl, 2.5 KCl, 26 NaHCO₃, 1 NaH₂PO₄, 2.5 CaCl₂, 1.3 MgSO₄, and 10 glucose equilibrated with 95% O₂/5% CO₂, pH 7.4. Slices were incubated in this solution for 30 min before recordings. For medial prefrontal cortex (mPFC) slices (300 μm thick), brain was cut in an ice-cold high-choline solution containing (in mM): 110 Choline-Cl, 2.5 KCl, 1.25 NaH₂PO₄, 7 MgCl₂, 25 NaHCO₃, 15 glucose, 0.5 CaCl₂, 11.6 ascorbate, 3.1 pyruvate (290–305 mmol/Kg) as previously described⁵⁷.

mPFC slices were kept at room temperature for at least 30 min before recording in ACSF containing (in mM): 124 NaCl, 2.69 KCl, 1.25 KH₂PO₄, 1.3 MgSO₄, 26 NaHCO₃, 10 glucose, 2.5 CaCl₂, pH 7.4 (300–305 mmol/Kg).

All experiments, except where indicated, were performed at 28 ± 1 °C in a submersion-type recording chamber perfused at 1–2 ml/min rate with ACSF supplemented with the GABAA receptor antagonist picrotoxin (PTX; 100 μM). Extracellular field potentials (fEPSPs) were recorded with a patch pipette filled with 1 mM NaCl and placed in the CA1 stratum radiatum. Whole-cell voltage-clamp recordings (Multiclamp 700B, Molecular Devices, USA) were acquired from CA1 pyramidal neurons or layer V pyramidal neurons voltage-clamped at -60 mV or +40 mV using patch pipette electrodes (3–4 M) containing the following intracellular solution (in mM): 131 Cs-gluconate, 8 NaCl, 1 CaCl₂, 10 EGTA, 10 glucose, 10 HEPES, pH 7.2, 292 mmol/kg osmolality. Reagents were obtained from Sigma, Tocris and Ascent Scientific, prepared in stock solutions and added to the ACSF as needed.

fEPSPs and excitatory postsynaptic currents (EPSCs) were evoked by stimulating Schaffer collateral inputs in the hippocampus and layer 2/3 in the mPFC with a monopolar electrode filled with ACSF and positioned ~100 to 150 μm away from the recording pipette. Miniature EPSCs (mEPSCs) were recorded at 32 ± 1 °C in the continuous presence of tetrodotoxin (TTX, 500 nM) to block action potential dependent release, whereas spontaneous EPSC (sEPSCs) were recorded in the absence of TTX. Short-term synaptic plasticity was induced by two pulses at different interstimulus interval (10, 30, 70, 100 and 300 ms) and were used to calculate paired-pulse ratio (PPR) that was defined as the ratio of the slope of the second fEPSP to the slope of the first fEPSP, respectively. Long-term potentiation (LTP) was induced by 4 trains of 100 pulses at 100 Hz repeated two times, separated by 10 s. The magnitude of LTP was compared with baseline 30–35 min after applying the stimulation protocol. To assess cell stability, series and input resistances were monitored with test pulses (-4 mV, 50 ms) throughout all experiments. Cells with >20% change in series resistance were excluded from analysis. All recordings were elicited at 15–20-s intervals, filtered at 2.4 kHz, and acquired at 10 kHz, using custom made software written in Igor Pro 6.36 (WaveMetrics). Statistical comparisons were made using two samples Student's t-test at $p < 0.05$ significance level, using Origin 8.5 Pro software (OriginLab). Unless otherwise indicated, all electrophysiological values are provided as mean ± S.E.M and illustrated traces are average of 31–40 responses.

Statistical analysis

Values are presented as mean ± standard error of mean (SEM) for 3 or more independent experiments. Statistical analyzes with Student's *t*-test or Two-samples student *t*-test was performed. Values of $p < 0.05$ were considered statistically significant. All statistical analyzes were performed using Graphpad Prism (GraphPad Software Inc.) or Origin 9.3 Pro (Origin Lab).

Data availability

All data supporting our conclusions are incorporated in the original manuscript. Other data and material are available from the corresponding authors upon request.

Received: 3 April 2024; Accepted: 20 August 2024

Published online: 02 September 2024

References

- Lord, C. *et al.* Autism spectrum disorder. *Nat. Rev. Dis. Prim.* **6**, 5 (2020).
- Parenti, I., Rabaneda, L. G., Schoen, H. & Novarino, G. Neurodevelopmental disorders: From genetics to functional pathways. *Trends Neurosci.* **43**, 608–621 (2020).
- Banerjee-Basu, S. & Packer, A. SFARI Gene: An evolving database for the autism research community. *Dis. Model Mech.* **3**, 133–135 (2010).
- Iossifov, I. *et al.* De novo gene disruptions in children on the autistic spectrum. *Neuron* **74**, 285–299 (2012).
- Rubeis, S. D. *et al.* Synaptic, transcriptional and chromatin genes disrupted in autism. *Nature* **515**, 209–215 (2014).
- Stessman, H. A. F. *et al.* Targeted sequencing identifies 91 neurodevelopmental-disorder risk genes with autism and developmental-disability biases. *Nat. Genet.* **49**, 515–526 (2017).
- Grove, J. *et al.* Identification of common genetic risk variants for autism spectrum disorder. *Nat. Genet.* **51**, 431–444 (2019).
- Ruzzo, E. K. *et al.* Inherited and de novo genetic risk for autism impacts shared networks. *Cell* **178**, 850–866.e26 (2019).
- Satterstrom, F. K. *et al.* Large-scale exome sequencing study implicates both developmental and functional changes in the neurobiology of autism. *Cell* **180**, 568–584.e23 (2020).
- Brauer, B., Merino-Veliz, N., Ahumada-Marchant, C., Arriagada, G. & Bustos, F. J. KMT2C knockout generates ASD-like behaviors in mice. *Front. Cell Dev. Biol.* **11**, 1227723 (2023).
- Platt, R. J. *et al.* Chd8 mutation leads to autistic-like behaviors and impaired striatal circuits. *Cell reports* **19**, 335–350 (2017).
- Tang, G.-B. *et al.* The histone H3K27 demethylase UTX regulates synaptic plasticity and cognitive behaviors in mice. *Front. Mol. Neurosci.* **10**, 267 (2017).
- Agger, K. *et al.* UTX and JMJD3 are histone H3K27 demethylases involved in HOX gene regulation and development. *Nature* **449**, 731–734 (2007).
- Cao, R. *et al.* Role of histone H3 lysine 27 methylation in polycomb-group silencing. *Science* **298**, 1039–1043 (2002).
- Nottke, A., Colaiácovo, M. P. & Shi, Y. Developmental roles of the histone lysine demethylases. *Development* **136**, 879–889 (2009).
- Burgold, T. *et al.* The histone H3 lysine 27-specific demethylase jmjd3 is required for neural commitment. *PLoS ONE* **3**, e3034 (2008).
- Wijayatunge, R. *et al.* The histone lysine demethylase Kdm6b is required for activity-dependent preconditioning of hippocampal neuronal survival. *Mol. Cell. Neurosci.* **61**, 187–200 (2014).
- Park, D. H. *et al.* Activation of neuronal gene expression by the JMJD3 demethylase is required for postnatal and adult brain neurogenesis. *Cell Rep.* **8**, 1290–1299 (2014).
- Shi, Y. Histone lysine demethylases: Emerging roles in development, physiology and disease. *Nat. Rev. Genet.* **8**, 829–833 (2007).
- Burgold, T. *et al.* The H3K27 demethylase JMJD3 is required for maintenance of the embryonic respiratory neuronal network, neonatal breathing, and survival. *Cell Rep.* **2**, 1244–1258 (2012).

21. Gao, Y., Aljazi, M. B. & He, J. Kdm6b haploinsufficiency causes ASD/ADHD-like behavioral deficits in mice. *Front. Behav. Neurosci.* **16**, 905783 (2022).
22. Ramesh, V., Liu, F., Minto, M. S., Chan, U. & West, A. E. Bidirectional regulation of postmitotic H3K27me3 distributions underlie cerebellar granule neuron maturation dynamics. *eLife* **12**, e86273 (2023).
23. Wang, Y. *et al.* KDM6B cooperates with Tau and regulates synaptic plasticity and cognition via inducing VGLUT1/2. *Mol. Psychiatry* **27**, 5213–5226 (2022).
24. Pineda, I. I. & González, C. L. G. The KDM6B mutation: Phenotype and clinical characteristics—Report of a case. *Rev. Psiquiatry Salud Ment.* **15**, 88–93 (2022).
25. Stolerman, E. S. *et al.* Genetic variants in the KDM6B gene are associated with neurodevelopmental delays and dysmorphic features. *Am. J. Méd. Genet. Part A* **179**, 1276–1286 (2019).
26. Rots, D. *et al.* The clinical and molecular spectrum of the KDM6B-related neurodevelopmental disorder. *Am. J. Hum. Genet.* **110**, 963–978 (2023).
27. Bustos, F. J. *et al.* Removal of a partial genomic duplication restores synaptic transmission and behavior in the MyosinVA mutant mouse Flailer. *BMC Biol.* **21**, 232 (2023).
28. Ahumada-Marchant, C. *et al.* Deletion of VPS50 protein in mouse brain impairs synaptic function and behavior. *BMC Biol.* **22**, 142 (2024).
29. Silverman, J. L., Yang, M., Lord, C. & Crawley, J. N. Behavioural phenotyping assays for mouse models of autism. *Nat. Rev. Neurosci.* **11**, 490–502 (2010).
30. Pandian, S. *et al.* Myosin va brain-specific mutation alters mouse behavior and disrupts hippocampal synapses. *eNeuro* **7**, ENEURO.0284-20.2020 (2020).
31. Pitts, M. Barnes maze procedure for spatial learning and memory in mice. *BIO-Protoc.* **8**, e2744 (2018).
32. Sepulveda, F. J. *et al.* Differential roles of NMDA receptor subtypes NR2A and NR2B in dendritic branch development and requirement of RasGRF1. *J. Neurophysiol.* **103**, 1758–1770 (2010).
33. Tindi, J. O. *et al.* ANKS1B gene product AIDA-1 controls hippocampal synaptic transmission by regulating GluN2B subunit localization. *J. Neurosci.* **35**, 8986–8996 (2015).
34. Paoletti, P., Bellone, C. & Zhou, Q. NMDA receptor subunit diversity: Impact on receptor properties, synaptic plasticity and disease. *Nat. Rev. Neurosci.* **14**, 383–400 (2013).
35. de la Torre-Ubieta, L., Won, H., Stein, J. L. & Geschwind, D. H. Advancing the understanding of autism disease mechanisms through genetics. *Nat. Med.* **22**, 345–361 (2016).
36. Wijayatunge, R. *et al.* The histone demethylase Kdm6b regulates a mature gene expression program in differentiating cerebellar granule neurons. *Mol. Cell. Neurosci.* **87**, 4–17 (2018).
37. Feliciano, P. *et al.* Exome sequencing of 457 autism families recruited online provides evidence for autism risk genes. *NPJ Genom Med.* **4**, 19 (2019).
38. Costa, V. *et al.* mTORC1 inhibition corrects neurodevelopmental and synaptic alterations in a human stem cell model of tuberous sclerosis. *Cell Rep.* **15**, 86–95 (2016).
39. Sacai, H. *et al.* Autism spectrum disorder-like behavior caused by reduced excitatory synaptic transmission in pyramidal neurons of mouse prefrontal cortex. *Nat. Commun.* **11**, 5140 (2020).
40. Budreck, E. C. *et al.* Neuroligin-1 controls synaptic abundance of NMDA-type glutamate receptors through extracellular coupling. *Proc. Natl. Acad. Sci.* **110**, 725–730 (2013).
41. Won, H. *et al.* Autistic-like social behaviour in Shank2-mutant mice improved by restoring NMDA receptor function. *Nature* **486**, 261–265 (2012).
42. Guang, S. *et al.* Synaptopathology involved in autism spectrum disorder. *Front. Cell. Neurosci.* **12**, 470 (2018).
43. van Zundert, B., Yoshii, A. & Constantine-Paton, M. Receptor compartmentalization and trafficking at glutamate synapses: A developmental proposal. *Trends Neurosci.* **27**, 428–437 (2004).
44. Bustos, F. J. *et al.* PSD95 suppresses dendritic arbor development in mature hippocampal neurons by occluding the clustering of NR2B-NMDA receptors. *PLoS ONE* **9**, e94037 (2014).
45. Elias, G. M., Elias, L. A. B., Apostolides, P. F., Kriegstein, A. R. & Nicoll, R. A. Differential trafficking of AMPA and NMDA receptors by SAP102 and PSD-95 underlies synapse development. *Proc. Natl. Acad. Sci. USA* **105**, 20953–20958 (2008).
46. Sans, N. *et al.* A developmental change in NMDA receptor-associated proteins at hippocampal synapses. *J. Neurosci.* **20**, 1260–1271 (2000).
47. Elias, G. M. *et al.* Synapse-specific and developmentally regulated targeting of AMPA receptors by a family of MAGUK scaffolding proteins. *Neuron* **52**, 307–320 (2006).
48. Henriquez, B. *et al.* Ezh1 and Ezh2 differentially regulate PSD-95 gene transcription in developing hippocampal neurons. *Mol. Cell. Neurosci.* **57**, 130–143 (2013).
49. Bustos, F. J. *et al.* Epigenetic editing of the Dlg4/PSD95 gene improves cognition in aged and Alzheimer's disease mice. *Brain* **140**, 3252–3268 (2017).
50. Rodenas-Ruano, A., Chávez, A. E., Cossio, M. J., Castillo, P. E. & Zukin, R. S. REST-dependent epigenetic remodeling promotes the developmental switch in synaptic NMDA receptors. *Nat. Neurosci.* **15**, 1382–1390 (2012).
51. Kim, J.-Y., Grunke, S. D., Levites, Y., Golde, T. E. & Jankowsky, J. L. Intracerebroventricular viral injection of the neonatal mouse brain for persistent and widespread neuronal transduction. *J. Vis. Exp.* **91**, 51863 (2014).
52. Passini, M. A. & Wolfe, J. H. Widespread Gene delivery and structure-specific patterns of expression in the brain after intraventricular injections of neonatal mice with an adeno-associated virus vector. *J. Virol.* **75**, 12382–12392 (2001).
53. Chan, K. Y. *et al.* Engineered AAVs for efficient noninvasive gene delivery to the central and peripheral nervous systems. *Nat. Neurosci.* **20**, 1172–1179 (2017).
54. Rein, B., Ma, K. & Yan, Z. A standardized social preference protocol for measuring social deficits in mouse models of autism. *Nat. Protoc.* **15**, 3464–3477 (2020).
55. Delgado-Acevedo, C. *et al.* Behavioral and synaptic alterations relevant to obsessive-compulsive disorder in mice with increased EAAT3 expression. *Neuropsychopharmacology* **44**, 1163–1173 (2019).
56. Plaza-Briceño, W. *et al.* N-Methyl-d-aspartate receptor modulation by nicotinamide adenine dinucleotide phosphate oxidase type 2 drives synaptic plasticity and spatial memory impairments in rats exposed pre- and postnatally to ethanol. *Antioxid. Redox Signal.* **32**, 602–617 (2020).
57. Cortés, B. I. *et al.* Loss of protein tyrosine phosphatase receptor delta PTPRD increases the number of cortical neurons, impairs synaptic function and induces autistic-like behaviors in adult mice. *Biol. Res.* **57**(1), 40 (2024).

Acknowledgements

This work was supported by: ANID Fondecyt Iniciacion 11180540 (FJB), ANID PAI 77180077 (FJB), Exploración-ANID 13220203 (FJB), ANID-MILENIO (NCN2023_32, FJB, LVN), UNAB DI-02-22/REG (FJB), Fond-equip EQM230028 (FJB), UNAB DI-06-24/REG (FJB), ANID-FONDECYT 1220480 (GA), ANID-FONDECYT 1201848 (A.E.C), ANID-FONDECYT 1230454 (LVN), DI-03-21/APP UNAB (BB), Fondecyt EQM160154

(A.E.C) and by ANID Millennium Science Initiative Program (P09-022F to A.E.C). R.C.M was supported by ANID-FONDECYT postdoctorado grant #3190793. CA-G and NM-V were supported by PhD fellowship from ANID #21201603 (to CA-G) and #21211967 (to NM-V).

Author contributions

B.B, N.M-V, and C.A-M performed all behavioral experiments and analyzed the results. C.A-G, and R.C.M performed all slices electrophysiological experiments and analyzed the results. F.J.B, G.N, L.V-N, G.A, and A.E.C designed experiments, guided the research, provided resources, and interpreted all the results. F.J.B, and A.E.C., wrote the paper.

Competing interests

The authors declare no competing interests.

Additional information

Supplementary Information The online version contains supplementary material available at <https://doi.org/10.1038/s41598-024-70728-5>.

Correspondence and requests for materials should be addressed to A.E.C. or F.J.B.

Reprints and permissions information is available at www.nature.com/reprints.

Publisher's note Springer Nature remains neutral with regard to jurisdictional claims in published maps and institutional affiliations.

Open Access This article is licensed under a Creative Commons Attribution-NonCommercial-NoDerivatives 4.0 International License, which permits any non-commercial use, sharing, distribution and reproduction in any medium or format, as long as you give appropriate credit to the original author(s) and the source, provide a link to the Creative Commons licence, and indicate if you modified the licensed material. You do not have permission under this licence to share adapted material derived from this article or parts of it. The images or other third party material in this article are included in the article's Creative Commons licence, unless indicated otherwise in a credit line to the material. If material is not included in the article's Creative Commons licence and your intended use is not permitted by statutory regulation or exceeds the permitted use, you will need to obtain permission directly from the copyright holder. To view a copy of this licence, visit <http://creativecommons.org/licenses/by-nc-nd/4.0/>.

© The Author(s) 2024